Active filter parameter tuning method for harmonic voltage mitigation in wind power plants

Li, Shuting; Wu, Jingxuan; Vasquez, Juan C.; Guerrero, Josep M.; Palensky, Peter; Lekić, Aleksandra

DOI
10.1016/j.epsr.2024.110726

Publication date
2024

Document Version
Final published version

Published in
Electric Power Systems Research

Electric Power Systems Research 234 (2024) 110726

Contents lists available at ScienceDirect

Electric Power Systems Research

journal homepage: www.elsevier.com/locate/epsr

Active filter parameter tuning method for harmonic voltage mitigation in wind power plants☆

Shuting Li [a,*], Jingxuan Wu [a], Juan C. Vasquez [a], Josep M. Guerrero [a,b,c], Peter Palensky [d], Aleksandra Lekić [d]

[a] AAU Energy, Aalborg University, 9220 Aalborg East, Denmark
[b] Department of Electronic Engineering, BarcelonaTech (UPC), 08019 Barcelona, Spain
[c] Catalan Institution for Research and Advanced Studies (ICREA), Pg. Lluís Companys 23, 08010 Barcelona, Spain
[d] Electrical Engineering, Mathematics and Computer Science, Delft University of Technology, 2628 CD Delft, Netherlands

ARTICLE INFO

Keywords:
Harmonic impedance reshaping
Harmonic modeling
Stability assessment

ABSTRACT

It is challenging to determine the active filter control factors in wind power plants (WPP) to obtain effective harmonic voltage mitigation and avoid over-modulation or system instability problems caused by overlarge feedforward or feedback gains. To address this issue, an active filter tuning (AFT) method is proposed in this paper to offer a common parameter tuning and stability assessment strategy for both current-controlled and voltage-controlled harmonic impedance reshaping (HIR) methods by introducing a coordination factor including different weight coefficients for system stability margin, wind turbine (WT) harmonic suppression, and grid harmonic mitigation. The superiority of the proposed method is verified in a 20 MW WPP with four cases considering both WT harmonic voltage amplification and grid voltage amplification. Compared to previous methods, the AFT-based HIR method achieves a more flexible balance between system stability and harmonic voltage mitigation, obtaining better performance in WT harmonic suppression, grid harmonic suppression, system robustness, and transient response.

1. Introduction

Grid compliance regarding power quality for wind power plants (WPP) poses additional challenges to utilities [1]. Harmonic mitigation of bus voltages and grid current is required for plant design and control operation. Compared with passive filters and additional active filter equipment [2,3], active filters implemented on stator-side converters of wind turbines (WT) reshape the converter output harmonic impedance in the control system, thereby more economical and effective [4]. These conventional converter harmonic output impedance reshaping (HIR) methods for renewable energy systems can be classified into current-controlled methods, voltage-controlled methods, and hybrid-controlled methods. The current-controlled methods suppress the WPP harmonics through the converter output current feedback [5–7], adding a virtual impedance on the converter equivalent harmonic output impedance. In voltage-controlled methods, the PCC voltage feedback [8] is adopted to suppress the harmonics coming from wind turbines or the grid, the unit PCC voltage feedforward [9] or capacitor voltage feedforward [10] are proposed to counteract the bus harmonic voltage provided by grid background harmonics. [11] proposes a voltage-controlled HIR method including a voltage feedforward branch and a voltage feedback branch, which can simultaneously suppress the grid harmonic current caused by WT and the grid. The hybrid methods [11–13] are the combination of the current and voltage control branches for harmonics mitigation. These HIR methods, however, require complex designing and parameter tuning procedures to avoid over-modulation or instability problems caused by overlarge feedforward or feedback gains [13].

In order to solve the above problem, [7] proposes a harmonic current sharing strategy to define the converter output current feedback gain according to the inverter's remaining available capacity. A one-order lead–lag filter proposed by [14] and a second-order phase-lead filter proposed by [15] are implemented on the PCC voltage feedforward branch to ensure the system stability in a strong grid with short circuit ratio (SCR) larger than 10. Paper [16] proposes an adaptive PCC voltage feedforward method to enhance the system robustness to

☆ Submitted to the 23rd Power Systems Computation Conference (PSCC 2024). This work was supported in part by the China Scholarship Council (CSC) and in part by the CRESYM project Harmony.

* Corresponding author.
E-mail addresses: shuli@energy.aau.dk (S. Li), jinwu@energy.aau.dk (J. Wu), juq@energy.aau.dk (J.C. Vasquez), joz@energy.aau.dk, josep.m.guerrero@upc.edu (J.M. Guerrero), P.Palensky@tudelft.nl (P. Palensky), A.Lekic@tudelft.nl (A. Lekić).

https://doi.org/10.1016/j.epsr.2024.110726
Received 28 September 2023; Received in revised form 10 March 2024; Accepted 17 June 2024
Available online 26 June 2024

grid impedance variation. Paper [17] proposes an output admittance shaping method for a current-controlled inverter to improve the WPP robustness to grid impedance variation according to the passivity-based stability criterion. Work [4] proposes an Extra Element Theorem-based virtual impedance tuning method according to impedance-based stability criterion. This method gives the optimal virtual impedance selection range to ensure effective harmonic voltage mitigation as well as enough stability margin, while the effect of wind turbine harmonics and grid background harmonics are not coordinately addressed. Furthermore, although the aforementioned methods enhance harmonic mitigation and system stability, most of them cannot be directly applied to type-III wind turbine systems because they lack the considerations of the dynamics of phase-locked loops (PLL) and rotor-side converter (RSC). This may result in an error in stability margin determination, posing additional uncertainties for harmonic mitigation strategy designing. In this sense, the parameter tuning and stability assessment of harmonic impedance reshaping for wind power plants need more attention.

Based on the research gap, an active filter tuning (AFT) method is proposed for harmonic voltage suppression in WPP to improve the harmonic suppression effect and the system stability. The main research contributions of this paper are as follows.

- The wind turbine (WT) sequence impedance model [18] is applied to the parameter tuning and stability assessment of harmonic impedance reshaping methods for WPP harmonic voltage mitigation. The sequence impedance model of type-III wind turbines considers the PLL perturbation, rotor machine impedance, rotor-side converter dynamics, and grid-side converter dynamics, giving accurate harmonic impedance modeling for harmonic mitigation [19].
- An AFT tuning method comprehensively addressing system stability margin, system transient performance, WT harmonics suppression, and grid harmonic mitigation is proposed to determine control factors of HIR methods. The AFT-based HIR methods effectively mitigate harmonic voltage at MV bus and PCC in WPP and simultaneously ensure adequate system stability margin by giving different weight coefficients for system stability, WT harmonic suppression, and grid harmonic suppression. Compared with previous methods, the proposed method offers enhanced flexibility in addressing both WT harmonic voltage amplification and grid harmonic voltage amplification according to the planning level. The AFT-based HIR method further demonstrates concurrent improvements in both harmonic suppression effect and system stability margin compared to the previous method.
- The proposed method offers a common tuning strategy for current-controlled and voltage-controlled HIR methods, breaking through the limitations of previous methods. Moreover, the proposed AFT can also be applied to other HIR methods for harmonic voltage suppression at all buses of WPP.

In the rest of the paper, the WPP architecture and sequence impedance modeling are introduced in Section 2. The proposed active filter tuning (AFT) method is discussed in Section 3. The case study and results of the proposed AFT method are presented in Section 4. Finally, the conclusions are given in Section 5.

2. WPP architecture and modeling

The typical single-line diagram of the WPP composed of type-III WTs is shown in Fig. 1. The type-III wind turbine feeds the grid side through a back-to-back converter. The wind turbine is connected to the MV bus through a transformer T1. The current flowing to the MV bus is scaled by N_t, representing that one single wind turbine is equivalent to N_t paralleled wind turbines [4]. A capacitor C representing the shunt capacitance of the cable collector is connected to the MV bus. The MV bus is connected to the PCC through a substation (SS) transformer T2.

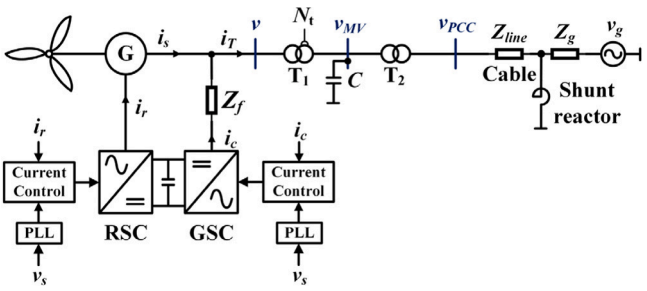

Fig. 1. Typical single-line structure of the grid-connected WPP composed of type-III wind turbines.

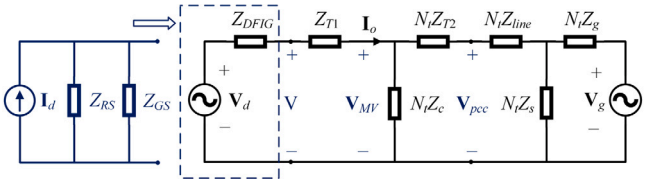

Fig. 2. Equivalent harmonic impedance model of the WPP.

The PCC is connected to the grid through the cables. The impedance of cables is modeled as a Π model including $R_{line}, L_{line}, C_R, C_L$ and represented as Z_{line}. $Z_g = R_{grid} + sL_{grid}$ denotes the internal impedance of the grid.

The RSC and GSC are controlled by the current controllers implemented at the d-q domain. Since the outer control loops to generate current references operate much slower than the inner current loops, the dynamics of these outer loops can be ignored [18]. In this sense, the equivalent harmonic impedance model can be developed in Fig. 2.

In Fig. 2, the grid background harmonics are modeled as a voltage source $\mathbf{V}_g$. Z_s represents the shunt reactor. The type-III wind turbine is modeled as a current disturbance source $\mathbf{I}_d$ paralleled with a rotor side impedance Z_{RS} and a grid side impedance Z_{GS} [18,19], which can be equivalent to a voltage disturbance source $\mathbf{V}_d$ in series with the total wind turbine impedance Z_{DFIG}. The disturbance source $\mathbf{V}_d$ represents the harmonic components coming from non-ideal PWM of converters i.e. dead-time and pulse deletion [4]. The Z_{RS} includes the rotor machine impedance and the impedance provided by the RSC controller, which is presented as [18].

$$Z_{RSp}(s) = \frac{sL_{sr} + R_s + \frac{R'_r}{\sigma_p(s)} + \frac{N_s^2}{N_r^2}\frac{H_{ri}(s-j\omega_1)-jK_{rd}}{\sigma_p(s)}}{1 - \frac{T_{PLL}(s-j\omega_1)}{2}\left[\frac{\mathbf{I}_{r1}}{\mathbf{V}_1}\frac{N_s^2}{N_r^2}\frac{H_{ri}(s-j\omega_1)-jK_{rd}}{\sigma_p(s)} + \frac{\mathbf{V}_{rs}}{\mathbf{V}_1}\right]} \tag{1}$$

$$Z_{RSn}(s) = \frac{sL_{sr} + R_s + \frac{R'_r}{\sigma_n(s)} + \frac{N_s^2}{N_r^2}\frac{H_{ri}(s+j\omega_1)+jK_{rd}}{\sigma_n(s)}}{1 - \frac{T_{PLL}(s+j\omega_1)}{2}\left[\frac{\mathbf{I}^*_{r1}}{\mathbf{V}^*_1}\frac{N_s^2}{N_r^2}\frac{H_{ri}(s+j\omega_1)+jK_{rd}}{\sigma_n(s)} + \frac{\mathbf{V}^*_{rs}}{\mathbf{V}^*_1}\right]}, \tag{2}$$

where the variables with the subscript p refer to the positive sequence components, the variables with the subscript n denote the negative sequence components, the subscript 1 represents the steady-state value of the vectors, $s = j\omega$ and

$$L_{sr} = L_s + L_r N_s^2/N_r^2, R'_r = R_r N_s^2/N_r^2 \tag{3}$$

$$\sigma_p(s) = (s - j\omega_m)/s, \sigma_n(s) = (s + j\omega_m)/s \tag{4}$$

$$H_{ri}(s) = K_{rp} + K_{ri}/s \tag{5}$$

$$T_{PLL}(s) = \frac{V_1(K_{pPLL} + K_{iPLL}/s)/s}{1 + V_1(K_{pPLL} + K_{iPLL}/s)/s} \tag{6}$$

$$\mathbf{V}_{rs} = \mathbf{V}_1 + \mathbf{I}_{r1}[j\omega_1 L_{sr} + R_s + R_r'/\sigma_p(j\omega_1)]. \tag{7}$$

In (1) and (2), the superscript * represents the conjugate complex of the variables. The impedance Z_{GS} provided by the GSC controller is presented as [20]

$$Z_{GSp}(s) = \frac{Z_f(s) + H_{si}(s - j\omega_1) - jK_{sd}}{1 - \frac{T_{PLL}(s-j\omega_1)}{2}\{\frac{\mathbf{I}_{c1}}{\mathbf{V}_1}[H_{si}(s - j\omega_1) - jK_{rd}] + \frac{\mathbf{V}_{gs}}{\mathbf{V}_1}\}} \tag{8}$$

$$Z_{GSn}(s) = \frac{Z_f(s) + H_{si}(s + j\omega_1) + jK_{sd}}{1 - \frac{T_{PLL}(s+j\omega_1)}{2}\{\frac{\mathbf{I}_{c1}^*}{\mathbf{V}_1^*}[H_{si}(s + j\omega_1) + jK_{rd}] + \frac{\mathbf{V}_{gs}^*}{\mathbf{V}_1^*}\}}, \tag{9}$$

where

$$H_{si}(s) = K_{sp} + K_{si}/s \tag{10}$$

$$\mathbf{V}_{gs} = \mathbf{V}_1 + \mathbf{I}_{c1} Z_f(j\omega_1). \tag{11}$$

In this way, the positive sequence wind turbine impedance Z_{DFIGp} can be obtained by connecting Z_{RSp} in (1) in parallel with Z_{GSp} in (8), the negative sequence impedance Z_{DFIGn} can be obtained by connecting Z_{RSn} in (2) in parallel with Z_{GSn} in (9). The control bandwidth of the GSC current controller is 400 Hz, and the L filter is adopted for impedance analysis in this paper. [18] has proved that the total WT positive impedance Z_{DFIGp} is mainly decided by the Z_{RSp} in sub-synchronous and super-synchronous bands; In the mid-band (100 Hz~400 Hz), the Z_{DFIGp} is mainly decided by Z_{RSp} and Z_{GSp}; And in the high-frequency band (>450 Hz), the Z_{DFIGp} is mainly decided by Z_{fp}. At main harmonic frequencies (eg. $-\omega_1$, $-5\omega_1$, $7\omega_1$), the Z_{DFIG} cannot be simplified to Z_{GS} or Z_{fp} due to the large magnitude and phase error between them. In this sense, the impedance analysis for WT using Z_{GS} is not accurate for harmonic impedance modeling of the WPP.

3. The proposed active filters tuning strategy

3.1. Impedance model of WPP with harmonic impedance reshaping

The harmonic impedance model of the WPP with two typical HIR methods is given in Fig. 3. In this figure, the HIR methods extract the harmonic component of $\mathbf{I}_o$ or $\mathbf{V}_{PCC}$ through the reduced-order generalized integrator (ROGI) G_h to form an additional harmonic source added on the GSC controller, increasing the total harmonic impedance viewed from the buses to the WT, correspondingly suppress harmonic voltages of the MV bus and PCC. The G_h is presented as [21]

$$G_h(s) = \sum_{h=-1,-5,7,-11,13,-17,19} \frac{K_r\omega_c}{s - j\omega_h + \omega_c}, \tag{12}$$

where K_r denotes the resonant gain of ROGI; the ω_c represents the cut-off frequency; $\omega_h = h\omega_1$ is the h order harmonic frequency.

According to Figs. 2 and 3, the contributions of the WT disturbance and grid background harmonics to MV bus harmonic voltage and PCC harmonic voltage can be obtained as

$$\mathbf{V}_b = A_{b,y}(s)\mathbf{V}_d + B_{b,y}(s)\mathbf{V}_g, \tag{13}$$

where b represents the buses i.e. b in $\{MV, PCC\}$, y represents the HIR control factors i.e. y in $\{0, Z_h, x\}$, A denotes the contribution of $\mathbf{V}_d$ to $\mathbf{V}_b$, and B denotes the contribution of $\mathbf{V}_g$ to $\mathbf{V}_b$. Note that the harmonic components V_d and V_g can be regarded as constant harmonic sources for harmonic impedance modeling [4,11]. When the HIR methods are not applied i.e. $y = 0$,

$$A_{MV,0}(s) = \frac{Z_c N_t Z_{Tg}}{Z_{total,0}}, B_{MV,0}(s) = \frac{Z_c Z_{out}}{Z_{total,0}} \frac{V_{eqg}}{V_g} \tag{14}$$

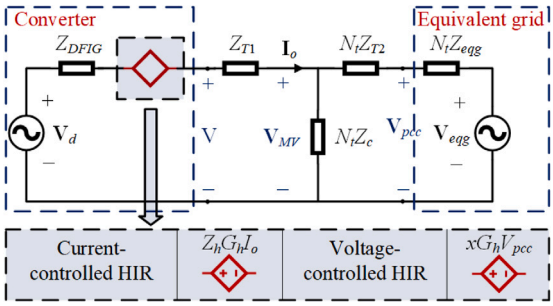

Fig. 3. Equivalent harmonic model of WPP with typical harmonic impedance reshaping methods.

$$A_{PCC,0}(s) = \frac{Z_c N_t Z_{eqg}}{Z_{total,0}}, B_{PCC,0}(s) = \frac{Z_c Z_{out} + (N_t Z_c + Z_{out})Z_{T2}}{Z_{total,0}} \frac{V_{eqg}}{V_g}, \tag{15}$$

where

$$Z_{total,0}(s) = Z_c Z_{out} + Z_{out} Z_{Tg} + Z_c N_t Z_{Tg}, \tag{16}$$

$Z_{out}(s) = Z_{DFIG} + Z_{T1}$, and $Z_{Tg} = Z_{T2} + Z_{eqg}$. Note that the Z_{eqg} and the $\mathbf{V}_{eqg}$ are the Thevenin equivalent model of cables, shunt reactor, and the grid. When the current-controlled HIR method is applied i.e. $y = Z_h$,

$$A_{MV,Z_h}(s) = \frac{Z_c N_t Z_{Tg}}{Z_{total,Z_h}}, \tag{17}$$

$$B_{MV,Z_h}(s) = \frac{Z_c(Z_{out} + Z_h G_h)}{Z_{total,Z_h}} \frac{V_{eqg}}{V_g} \tag{18}$$

$$A_{PCC,Z_h}(s) = \frac{Z_c N_t Z_{eqg}}{Z_{total,Z_h}} \tag{19}$$

$$B_{PCC,Z_h}(s) = \frac{Z_c(Z_{out} + Z_h G_h) + (N_t Z_c + Z_h G_h + Z_{out})Z_{T2}}{Z_{total,Z_h}} \frac{V_{eqg}}{V_g}, \tag{20}$$

where

$$Z_{total,Z_h}(s) = Z_{total,0} + Z_h G_h(Z_{Tg} + Z_c). \tag{21}$$

When the voltage-controlled HIR method is applied i.e. $y = x$,

$$A_{MV,x}(s) = \frac{Z_c N_t Z_{Tg}}{Z_{total,x}}, \tag{22}$$

$$B_{MV,x}(s) = \frac{Z_c Z_{out} - Z_c x G_h N_t Z_{T2}}{Z_{total,x}} \frac{V_{eqg}}{V_g} \tag{23}$$

$$A_{PCC,x}(s) = \frac{Z_c N_t Z_{eqg}}{Z_{total,x}}, \tag{24}$$

$$B_{PCC,x}(s) = \frac{Z_c Z_{out} + Z_{total,0} Z_{T2}/Z_{Tg}}{Z_{total,x}} \frac{V_{eqg}}{V_g} \tag{25}$$

Where

$$Z_{total,x}(s) = Z_{total,0} + x G_h Z_c N_t Z_{eqg} \tag{26}$$

Define the suppression effects of HIR methods on the converter harmonics and the grid background harmonics are

$$SF_{A,b,y}(s) = |\frac{A_{b,y}}{A_{b,0}}|, SF_{B,b,y}(s) = |\frac{B_{b,y}}{B_{b,0}}|, \tag{27}$$

respectively. When the suppression factors $SF_{A,b,y}$ and $SF_{B,b,y}$ are both less than 1, the HIR methods can be regarded as effective in suppressing the harmonic voltages of MV bus and PCC in WPP. To

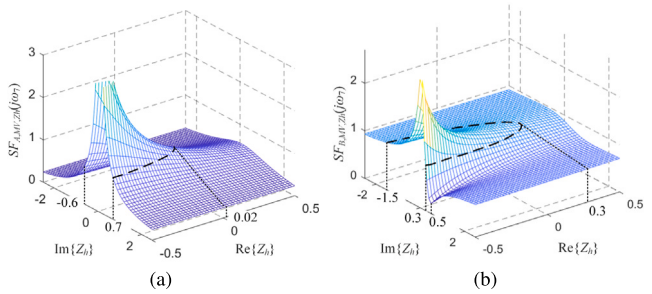

Fig. 4. Voltage suppression factor at the MV bus with the current-controlled HIR.(a) Factor result due to WT harmonics. (b) Factor result due to the grid harmonics.

analyze the impact of the HIR control factors i.e. Z_h, x on the harmonic voltage suppression performance, consider the suppression factor SF_{A,MV,Z_h}, SF_{B,MV,Z_h} at 7_{th} harmonic. Fig. 4 shows the bode diagram of $SF_{A,MV,Z_h}(j7\omega_1)$, $SF_{B,MV,Z_h}(j7\omega_1)$ with different complex values of Z_h. In Fig. 4(a)(b), the area where suppression factor SF_{A,MV,Z_h} and SF_{B,MV,Z_h} are larger than 1 indicates that the harmonic components of the bus voltages will be increased with these Z_h values due to the reduction of the overall impedance viewed from the MV bus to the converter and the impedance viewed from PCC to the converter. In Fig. 4(a), the ideal harmonic suppression effect on $\mathbf{V}_{MV}/\mathbf{V}_d$ is provided by $|\mathrm{Im}\{Z_h\}| > 0.7$, and this effect is improved as the $|\mathrm{Im}\{Z_h\}|$ increases. In Fig. 4(b), the optimal harmonic suppression effect on $\mathbf{V}_{MV}/\mathbf{V}_g$ is provided by $Z_h = -0.5 + j0.5$, and this effect is weakened as the $\mathrm{Im}\{Z_h\}$ increases. The effect of Z_h on $\mathbf{V}_{MV}/\mathbf{V}_d$ and $\mathbf{V}_{MV}/\mathbf{V}_g$ is counteracted when $\mathrm{Im}\{Z_h\} > 0.5$. Note that this phenomenon not only occurs at the 7_{th} harmonic, but also occurs at other order harmonics. This is because the Z_h only affects the denominator of SF_{A,MV,Z_h} but introduces additional gain on the numerator of SF_{B,MV,Z_h}. In this sense, the contributions of $\mathbf{V}_d$ and $\mathbf{V}_g$ should be coordinately considered to determine the appropriate control factor values of HIR methods.

3.2. Stability analysis of HIR gains

In a WPP, stability is another important design indicator for HIR methods. The overlarge feedforward or feedback gains of HIR methods may cause over-modulation or instability problems in the system. In this sense, Z_h and x should be designed first to ensure the system stability, as investigated in [1,13]. Accordingly, the stability margin of the WPP depending on the system impedance offers additional value restrictions on HIR gains. According to the impedance-based stability criterion [22] and Fig. 3, the system stability is decided by $H_y(s)$ when the original system without HIR methods is stable, where

$$H_y(s)|_{y=Z_h} = \frac{Z_{total,0}}{Z_{total,Z_h}} = \frac{1}{1 + Z_h(s)G_h(s)/[Z_{out} + Nt(Z_c//Z_{Tg})]}, \tag{28}$$

$$H_y(s)|_{y=x} = \frac{Z_{total,0}}{Z_{total,x}} = \frac{1}{1 + \frac{xG_hZ_cN_tZeqg}{Z_{total,0}}}. \tag{29}$$

In (28) and (29), $H_y(s)$ resembles the closed-loop transfer function of the feedback control system with the current-controlled HIR method and voltage-controlled HIR method. When the system feedback gain satisfies the Nyquist stability criterion, it is possible to define the stability margin of the system as [23]

$$\eta_y = \min_{-\infty \leqslant \omega \leqslant +\infty} |\mathrm{den}(H_y(j\omega))|. \tag{30}$$

η_y represents the minimum distance of the system feedback gain from the critical point (−1, j0). When the system feedback gain does not satisfy the Nyquist stability criterion, this distance η_y is defined as 0. The optimal ranges for this η_y value is $[0.5, 0.8]$. Systems with this stability margin will ensure a good transient response as well as enough robustness to grid impedance variation [24].

3.3. HIR parameters tuning strategy

Based on the above analysis and definition, the ideal HIR method for h order harmonics suppression should meet three conditions: (1) $SF_{A,b,y}(j\omega_h) < 1$, and the smaller the better. (2) $SF_{B,b,y}(j\omega_h) < 1$, and the smaller the better. (3) $0.5 \leqslant \eta_y \leqslant 0.8$. However, sometimes it is difficult to find a value that satisfies these three conditions at the same time if the harmonic distortion is serious. In this sense, a coordination strategy is proposed to balance these three conditions and provide the appropriate value ranges for HIR control factors to obtain optimal system stability as well as harmonic suppression effect on MV bus voltage and PCC voltage.

For different buses i.e. MV bus and PCC, the contribution of $\mathbf{V}_d$ or $\mathbf{V}_g$ is different. If a control factor value cannot be found to obtain the smallest $SF_{A,b,y}$ and $SF_{B,b,y}$ simultaneously, the coordination tuning strategy should make the best choice to minimize $\mathbf{V}_b$ and ensure the system stability margin. Accordingly, a performance index to indicate favorable Z_h and x values can be formulated as

$$CF_{b,y}(j\omega_h) = \frac{\eta_y}{m_bSF_{A,b,y}(j\omega_h) + n_bSF_{B,b,y}(j\omega_h)}, \eta_y < k$$

$$CF_{b,y}(j\omega_h) = \frac{k}{m_bSF_{A,b,y}(j\omega_h) + n_bSF_{B,b,y}(j\omega_h)}, \eta_y \geq k \tag{31}$$

where k is a user-designed control factor to obtain best performance on system stability margin and harmonic suppression effects. m_b and n_b are the weight coefficients for $SF_{A,b,y}(j\omega_h)$ and $SF_{B,b,y}(j\omega_h)$, respectively. The m_b and n_b can be defined as

$$m_b = \frac{|A_{b,0}(j\omega_h)|}{|A_{b,0}(j\omega_h)| + |B_{b,0}(j\omega_h)|} \tag{32}$$

$$n_b = \frac{|B_{b,0}(j\omega_h)|}{|A_{b,0}(j\omega_h)| + |B_{b,0}(j\omega_h)|}. \tag{33}$$

In (31), the performance of an HIR method is valued on the system stability, the WT harmonics suppression, and the grid background harmonics suppression. Larger $CF_{b,y}(j\omega)$ indicates smaller $SF_{A,b,y}(j\omega_h)$, smaller $SF_{B,b,y}(j\omega_h)$, and better η_y. Take the MV bus with the current-controlled HIR method as an example for analysis. When the harmonics generated by WTs have a greater impact on the $\mathbf{V}_{MV}$ at h order harmonic frequency due to the shorter transmission cables or voltage amplification of WT harmonics, i.e. $|A_{MV,0}(j\omega)| > |B_{MV,0}(j\omega)|$, the weight coefficient m_b will be larger than n_b. In this way, a Z_h value obtaining smaller $SF_{A,MV,Z_h}(j\omega)$ will result in a larger $CF_{MV,Z_h}(j\omega)$ value rather than a Z_h value obtaining smaller $SF_{B,MV,Z_h}(j\omega)$. The system with the current-controlled HIR method will accordingly put more effort into addressing the harmonics generated by WTs. Similarly, when $|B_{MV,0}(j\omega)|$ is largely increased due to the parallel resonance in the transmission grid, the weight coefficient n_b will be much larger than m_b. In this way, the HIR method will mainly address the harmonics caused by the grid. In (31), when the system stability margin η_y is less than k, the optimal Z_h value will be produced by a larger stability margin. When the η_y is larger than k, the weight of the stability margin will be fixed to k. Note that this weight value k is determined by the planning level of the voltage harmonics. In this sense, the system can be dedicated to finding smaller values of $SF_{A,MV,Z_h}(j\omega)$ and $SF_{B,MV,Z_h}(j\omega)$ with a sufficient system stability margin. The detailed AFT calculation procedures for the HIR methods are as follows:

(1) Determine the harmonic frequency ω_h of the voltage harmonic and the bus b to be controlled. Determine the HIR control factor y to be used.

(2) Let $b = \mathrm{Re}\{b\} + j\mathrm{Im}\{b\}$ be the independent variables. Set $k = 0.65$, which is the average value of the optimal stability margin range [0.5,0.8].

(3) Calculate $CF_{b,y}(\mathrm{Re}\{b\}, \mathrm{Im}\{b\})$ in (31) accordingly.

Table 1
Studied cases.

Cases	V_d amplification	V_g amplification	Planning level
Case I	√	√	$SF_{A,MV} = 0.5$
Case II	×	×	$SF_{A,MV} = 0.3$
Case III	√	×	$SF_{A,MV} = 0.3$
Case IV	×	√	$SF_{B,MV} = 0.5$

(4) Perform global optimization on $CF_{b,y}(\mathrm{Re}\{b\},\mathrm{Im}\{b\})$ to find the maximum point $CF_{b,y,max}(\mathrm{Re}\{b,m\},\mathrm{Im}\{b,m\})$.

(5) Check if the $SF_{A,b,y}(\mathrm{Re}\{b,m\},\mathrm{Im}\{b,m\})$ and $SF_{B,b,y}(\mathrm{Re}\{b,m\},\mathrm{Im}\{b,m\})$ in (27) satisfy the harmonic planning level.

(6) If the planning level is satisfied, output $\mathrm{Re}\{b,m\}$, $\mathrm{Im}\{b,m\}$, $SF_{A,b,y}(\mathrm{Re}\{b,m\},\mathrm{Im}\{b,m\})$, $SF_{B,b,y}(\mathrm{Re}\{b,m\},\mathrm{Im}\{b,m\})$, and $\eta_y(\mathrm{Re}\{b,m\},\mathrm{Im}\{b,m\})$.

(7) If the planning level is not satisfied, let $k = k - 0.1$ and repeat steps 3 to 7 until $k = 0.15$.

In this way, the proposed AFT method can flexibly balance between sufficient system stability margin and satisfactory harmonic voltage suppression for the WPP.

4. Case study and results

This section presents results of the proposed AFT method based on a running example in [19] involving a 20 MW WPP with the structure in Fig. 1. The WPP is composed of 10 Type-III wind turbines with 2 MW rated capacity each. The WTs are connected to the MV bus through the 690V/32 kV transformers, and the MV bus is connected to the PCC by a 32 kV/110 kV transformer T2. The scale factor N_t is 10. The other parameters for the WPP are listed in Table 2. Results in this section are obtained by MATLAB calculation. Since the above two typical HIR methods are more effective in suppressing the MV bus harmonic voltage, the following analysis will be based on the MV bus harmonic voltage suppression. The AFT-based HIR methods are implemented in four cases as Table 1 to verify the superiority of the proposed method.

Case I and Case II simulate the WPP with both WT harmonics amplification and grid harmonics amplification or the WPP with neither WT harmonics amplification nor grid harmonics amplification existing. According to the WPP parameters, the impact of $\mathbf{V}_d$ on $\mathbf{V}_{MV}$ is $A_{MV,0} = 0.6$ and the impact of $\mathbf{V}_g$ on $\mathbf{V}_{MV}$ is $B_{MV,0} = 0.38$. For the MV bus harmonic voltage suppression, the planning level of SF_{A,MV,Z_h} is set to be 0.5 in Case I, and 0.3 in Case II. Case III simulates the WPP with only WT harmonics amplification exists and the planning level is $SF_{A,MV,Z_h} = 0.3$. Case IV simulates the WPP with only grid harmonics amplification existing when the planning level is $SF_{B,MV,Z_h} = 0.5$.

4.1. Results of AFT for current-controlled HIR method

Fig. 5 shows AFT results in Case I and Case II. In these cases, the m_{z_h} is slightly larger than n_{z_h}, and the AFT mainly reduces the SF_{A,MV,Z_h} to suppress the harmonics resulting from WT converters. In this way, the optimal harmonic suppression performance is obtained by $Z_h = 0.8+j0.8$ in Fig. 5(a) in Case I. The corresponding harmonic suppression effect SF_{A,MV,Z_h} is 0.39, SF_{B,MV,Z_h} is 0.74, and the phase margin η_{Z_h} is 0.74. With this Z_h value, the harmonic suppression on $\mathbf{V}_{MV}$ satisfies the planning level, and the system margin is within the optimal range [0.5,0.8]. As shown in Fig. 5(b), the $Z_h = 0.8 + j1.8$ offers the best harmonic suppression performance in Case II. The corresponding harmonic suppression effect SF_{A,MV,Z_h} is 0.27, SF_{B,MV,Z_h} is 0.71, and the phase margin η_{Z_h} is 0.27. With this Z_h value, the AFT-based HIR effectively reduces the $\mathbf{V}_{MV}/\mathbf{V}_d$ to 0.27 times the original value. Although the system phase margin is reduced to 0.27, the system remains stable. The system sacrifices part of the stability margin to reduce the MV bus harmonics to be below the planning level. Note that results in these two cases are also valid in the situation where both WT harmonic amplification and grid harmonic amplification exist.

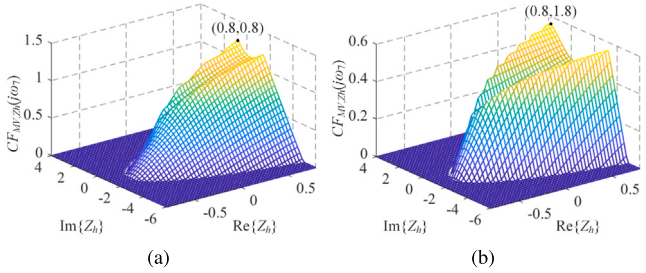

Fig. 5. AFT-based current controlled HIR results for MV bus harmonic voltage suppression. (a) Result in Case I. (b) Result in Case II.

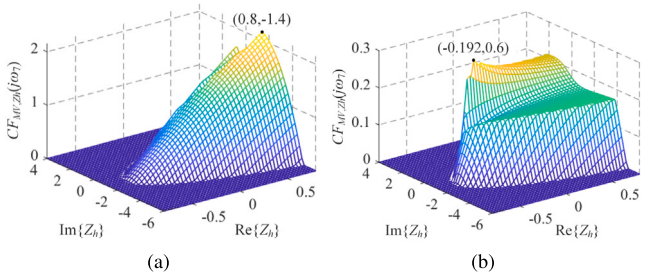

Fig. 6. AFT-based current controlled HIR results for MV bus harmonic voltage suppression. (a) Result in Case III. (b) Result in Case IV.

When a large voltage amplification of WT harmonics occurs alone in the WPP, the weight coefficient m_{Z_h} will be accordingly increased to be much larger than n_{Z_h}. In this sense, the weight coefficient n_{Z_h} is set as 0 in case III to simulate the large voltage amplification of WT harmonics in WPP. The system with AFT thus only focuses on reducing $A_{MV,Zh}$. In case IV, the $\mathbf{V}_{eqg}$ is regarded as an independent harmonic source. The impact of $\mathbf{V}_{eqg}$ on $\mathbf{V}_{MV}$ is $B_{MV,0} = 4$, showing an amplification of grid voltage harmonics is occurring alone. In this sense, the AFT is dedicated to suppressing the grid background harmonics. Fig. 6 presents the AFT-based current-controlled HIR results in these two cases. In Fig. 6(a), the AFT-based HIR offers best harmonic suppression performance on $\mathbf{V}_{MV}/\mathbf{V}_d$ with $Z_h = 0.8 - j1.4$. The corresponding harmonic suppression effect SF_{A,MV,Z_h} is 0.3, SF_{B,MV,Z_h} is 0.9, and the phase margin η_{Z_h} is 0.65. The AFT-based HIR effectively suppresses the harmonic voltage caused by WT harmonics to planning level 0.3 and not amplifies the harmonic voltage caused by grid harmonics. Moreover, the system stability remains within the optimal range. As shown in Fig. 6(b), the AFT-based HIR offers best harmonic suppression performance on $\mathbf{V}_{MV}/\mathbf{V}_g$ with $Z_h = -0.192 + j0.6$. The corresponding harmonic suppression effect SF_{A,MV,Z_h} is 0.9, SF_{B,MV,Z_h} is 0.5, and the phase margin η_{Z_h} is 0.16. The AFT-based HIR effectively reduces the $\mathbf{V}_{MV}/\mathbf{V}_g$ to the planning level 0.5. Although the system robustness is largely reduced with extreme voltage amplification, the system with AFT-based HIR can still obtain effect harmonic voltage suppression and ensure the system stability.

4.2. Comparison results with previous method

As reviewed in the Introduction, an EET-based active filter tuning (EAF) method is proposed in [4] to determine the optimal value of the abovementioned current-controlled HIR method. In order to verify the superiority of the proposed AFT method, the comparative simulations are also implemented in Case III and Case IV with the EAF method.

Table 2
Studied WPP parameters.

Component	Parameter	Value	Component	Parameter	Value	Component	Parameter	Value
RSC controller	$\mathbf{I}_{r1}$	$5.8\angle -22°$ A	GSC controller	$\mathbf{I}_{c1}$	$152.3\angle 114°$ A	Filter	L_f	1 mH
	K_{rp}	0.052		K_{sp}	1.452	DC voltage	V_{dc}	1200 V
	K_{ri}	0.027		K_{si}	3384	Sampling	f_s	12.8 kHz
	K_{rd}	0.00245		K_{sd}	0.025	PWM	f_{sw}	1950 Hz
Rotor	N_r	0.33	Stator	N_s	1	WT transformer	R_{wtt}	2.57 Ω
	R_r	0.0092 Ω		R_s	0.0092 Ω		L_{wtt}	68.26 mH
	L_r	0.0644 mH		L_s	0.1356 mH	SS transformer	R_{sst}	0.249 Ω
	n_m	1080 rpm		p	3		L_{sst}	9.51 mH
PLL	K_{pPLL}	48.873	Cable	R_{line}	0.13 Ω/km	Grid	f_1	50 Hz
	K_{iPLL}	3070.1		L_{line}	0.356 mH/km		R_{grid}	7.015 Ω
	$\mathbf{V}_1$	$564.1\angle -59°$ V		C_L, C_R	0.25 μF/km		L_{grid}	2.23 mH

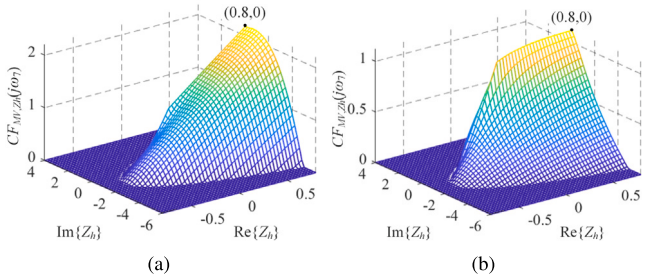

Fig. 7. EAF-based current controlled HIR results for MV bus harmonic voltage suppression. (a) Result in Case III. (b) Result in Case IV.

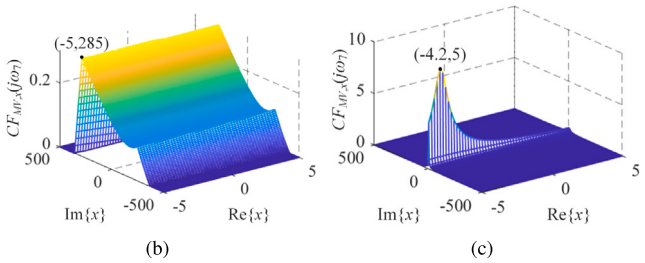

Fig. 8. AFT-based voltage controlled HIR results for MV bus harmonic voltage suppression. (a) Result in Case III. (b) Result in Case IV.

The results of EAF are presented in Fig. 7. Note that only the results of proposed AFT and EAF [4] in case III and case IV are compared, since the EAF only considers the situation where WT harmonic amplification exists alone or the grid harmonic amplification exists alone.

Fig. 7 shows the EAF results for MV bus harmonic voltage suppression in case III and case IV. In Fig. 7(a), the EAF offers best harmonic suppression performance on $\mathbf{V}_{MV}/\mathbf{V}_d$ with $Z_h = 0.8 + j0$. The corresponding harmonic suppression effect SF_{A,MV,Z_h} is 0.44, SF_{B,MV,Z_h} is 0.85, and the phase margin η_{Z_h} is 0.95. It is obvious the EAF fails to reduce the SF_{A,MV,Z_h} to the planning level 0.3 in case III. Moreover, the system stability margin with EAF is above the optimal range, representing the deterioration of the system transient performance. In Fig. 7(b), the EAF also offers best harmonic suppression performance on $\mathbf{V}_{MV}/\mathbf{V}_g$ with $Z_h = 0.8 + j0$. The corresponding harmonic suppression effect and the phase margin η_{Z_h} are the same as values in case III. The SF_{B,MV,Z_h} value 0.85 is much higher than the planning level 0.5, and the system transient performance deteriorates. Comparing Figs. 6 and 7, the proposed AFT method obtains better performance on harmonic voltage suppression and system stability improvement both in the situations where WT harmonic amplification exists alone and the grid harmonic amplification exists alone.

4.3. Results of AFT for voltage-controlled HIR method

The voltage-controlled HIR method in Fig. 3 is proposed to be applied in Case III and Case IV. There is no value of control factor x to make this method applied in both WT harmonics suppression and grid harmonics suppression. In this sense, only results of AFT-based voltage-controlled HIR in Case III and Case IV are presented.

Fig. 8(a) shows the AFT-based voltage-controlled HIR result in Case III. The best harmonic suppression performance on $\mathbf{V}_{MV}/\mathbf{V}_d$ is provided by $x = -5 + j280$. The corresponding harmonic suppression effect $SF_{A,MV,x}$ is 0.48 and the phase margin η_x is 0.15. Although the $SF_{A,MV,x}$ value is above the planning level, the AFT still effectively reduces the $SF_{A,MV,x}$ to below 0.5. In Fig. 8(b), the best harmonic suppression performance on $\mathbf{V}_{MV}/\mathbf{V}_g$ is given by $x = -4.2 + j5$. The corresponding harmonic suppression effect $SF_{B,MV,x}$ is 0.06 and the phase margin η_x is 0.96. The harmonic suppression is effective since the $SF_{B,MV,x}$ value is much lower than the planning level. And the system stability is ensured. The voltage-controlled HIR method is more suitable for suppressing the harmonic voltage of the MV bus caused by grid background harmonics in the WPP.

5. Conclusion

The type-III WT sequence impedance model is employed to develop the harmonic model for WPPs. Based on the harmonic model, an active filter tuning method is proposed for parameter tuning and system stability analysis of WPPs controlled by HIR methods. The proposed AFT method offers a common tuning strategy for both current-controlled and voltage-controlled HIR methods, optimizing the determination of the harmonic control factors of HIR. With the AFT-based HIR methods, the WPP can effectively mitigate the bus harmonic voltages, ensuring system stability and transient performance. The superiority of the proposed method is verified in a WPP with four cases considering the voltage amplification of WT harmonics as well as the amplification of grid harmonics. Compared to the previous method, the proposed AFT obtains better performance in harmonic voltage suppression and system stability enhancement. Moreover, the proposed AFT can be applied to other HIR methods for harmonic voltage suppression at other buses.

CRediT authorship contribution statement

Shuting Li: Conceptualization, Methodology, Writing – original draft. **Jingxuan Wu:** Conceptualization, Methodology, Visualization. **Juan C. Vasquez:** Supervision, Writing – review & editing. **Josep M. Guerrero:** Resources, Supervision, Writing – review & editing. **Peter Palensky:** Supervision. **Aleksandra Lekić:** Funding acquisition, Supervision, Writing – review & editing.

Declaration of competing interest

The authors declare that they have no known competing financial interests or personal relationships that could have appeared to influence the work reported in this paper.

Data availability

No data was used for the research described in the article.

References

[1] X. Wang, F. Blaabjerg, Harmonic stability in power electronic-based power systems: Concept, modeling, and analysis, IEEE Trans. Smart Grid 10 (3) (2019) 2858–2870.

[2] L. Jia, X. Ruan, W. Zhao, Z. Lin, X. Wang, An adaptive active damper for improving the stability of grid-connected inverters under weak grid, IEEE Trans. Power Electron. 33 (11) (2018) 9561–9574.

[3] M. Lehmann, D.M. Pieschel, M. Juamparez, K. Kabel, D.Ł.H. Kocewiak, S. Sahukari, Active filtering in a large-scale STATCOM for the integration of offshore wind power, in: 17th International Wind Integration Workshop, 2018.

[4] E. Guest, K.H. Jensen, T.W. Rasmussen, Mitigation of harmonic voltage amplification in offshore wind power plants by wind turbines with embedded active filters, IEEE Trans. Sustain. Energy 11 (2) (2020) 785–794.

[5] Y. Han, P. Shen, X. Zhao, J.M. Guerrero, Control strategies for islanded microgrid using enhanced hierarchical control structure with multiple current-loop damping schemes, IEEE Trans. Smart Grid 8 (3) (2017) 1139–1153.

[6] F. Deng, X. Li, X. Zhang, P. Mattavelli, An iterative virtual impedance regulation strategy in islanded microgrids for enhanced balanced, unbalanced and harmonic current sharing, IEEE Trans. Sustain. Energy 13 (1) (2022) 514–526.

[7] P. Sreekumar, V. Khadkikar, Direct control of the inverter impedance to achieve controllable harmonic sharing in the islanded microgrid, IEEE Trans. Ind. Electron. 64 (1) (2017) 827–837.

[8] S.K. Chaudhary, C. Lascu, R. Teodorescu, L. Kocewiak, Voltage feedback based harmonic compensation for an offshore wind power plant, in: 2016 IEEE International Conference on Power Electronics, Drives and Energy Systems (PEDES), 2016, pp. 1–5.

[9] M. Hamzeh, H. Karimi, H. Mokhtari, Harmonic and negative-sequence current control in an islanded multi-bus MV microgrid, IEEE Trans. Smart Grid 5 (1) (2014) 167–176.

[10] A. Ghoshal, V. John, Active damping of LCL filter at low switching to resonance frequency ratio, IET Power Electron. 8 (4) (2015) 574–582.

[11] L. Zhou, Z. Shuai, Y. Chen, W. Wu, X. Zhou, K. Yan, A. Luo, Impedance-based harmonic current suppression method for VSG connected to distorted grid, IEEE Trans. Ind. Electron. 67 (7) (2020) 5490–5502.

[12] J. He, Y.W. Li, F. Blaabjerg, Flexible microgrid power quality enhancement using adaptive hybrid voltage and current controller, IEEE Trans. Ind. Electron. 61 (6) (2014) 2784–2794.

[13] T. Wang, H. Nian, Z.Q. Zhu, L. Ding, B. Zhou, Flexible compensation strategy for voltage source converter under unbalanced and harmonic condition based on a hybrid virtual impedance method, IEEE Trans. Power Electron. 33 (9) (2018) 7656–7673.

[14] Z. Lin, Z. Chen, L. Yajuan, L. Bin, L. Jinhong, X. Bao, Phase-reshaping strategy for enhancing grid-connected inverter robustness to grid impedance, IET Power Electron. 11 (8) (2018) 1434–1443.

[15] X. Chen, Y. Zhang, S. Wang, J. Chen, C. Gong, Impedance-phased dynamic control method for grid-connected inverters in a weak grid, IEEE Trans. Power Electron. 32 (1) (2017) 274–283.

[16] J. Xu, S. Xie, Q. Qian, B. Zhang, Adaptive feedforward algorithm without grid impedance estimation for inverters to suppress grid current instabilities and harmonics due to grid impedance and grid voltage distortion, IEEE Trans. Ind. Electron. 64 (9) (2017) 7574–7586.

[17] Q. Qian, S. Xie, J. Xu, S. Bian, N. Zhong, Passivity-based output admittance shaping of the converter-side current-controlled grid-tied inverter to improve the robustness to the grid impedance, IET Power Electron. 13 (10) (2020) 1956–1965.

[18] I. Vieto, J. Sun, Sequence impedance modeling and analysis of type-III wind turbines, IEEE Trans. Energy Convers. 33 (2) (2018) 537–545.

[19] H. Ghanavati, L.u.H. Kocewiak, A. Jalilian, O. Gomis-Bellmunt, Transfer function-based analysis of harmonic and interharmonic current summation in type-III wind power plants using DFIG sequence impedance modeling, Electr. Power Syst. Res. 199 (2021) 107419.

[20] M. Cespedes, J. Sun, Impedance modeling and analysis of grid-connected voltage-source converters, IEEE Trans. Power Electron. 29 (3) (2014) 1254–1261.

[21] C. Xie, X. Zhao, K. Ki, D. Liu, J.M. Guerrero, J.C. Vasquez, Phase compensated reduced order generalized integrators for grid-tied VSCs with harmonics compensation capability, IEEE Trans. Ind. Appl. 54 (3) (2018) 2568–2578.

[22] J. Sun, Impedance-based stability criterion for grid-connected inverters, IEEE Trans. Power Electron. 26 (11) (2011) 3075–3078.

[23] A.G. Yepes, Analysis and design of resonant current controllers for voltage-source converters by means of nyquist diagrams and sensitivity function, IEEE Trans. Ind. Electron. 58 (11) (2011) 20.

[24] K.J. Åström, R.M. Murray, Feedback Systems: An Introduction for Scientists and Engineers, Princeton University Press, 2021,